# Supporting Information

**Microstructure Engineering of Fe/$Fe_3C$-Decorated Metal-Nitrogen-Carbon Mesoporous Nanospheres via a Self-Template Method for Enhancing Oxygen Reduction Activity**

Wanxin She,[a, ǁ] Qianru Xie,[a, ǁ] Yaohui Huang,[b] Chuyi Xie,[a] Xiangyu Zhang,[a] Mingchen Sun,[a] Feng Wang,[a] Junwu Xiao,[a,*]

[a]Key Laboratory of Material Chemistry for Energy Conversion and Storage, Ministry of Education, Hubei Key Laboratory of Material Chemistry and Service Failure, Department of Chemistry and Chemical Engineering, Huazhong University of Science & Technology, Wuhan, PR China

[b]school of life sciences, Central China Normal University, Wuhan, PR China

*E-mail: chjwxiao@hust.edu.cn

[ǁ]They contribute equally to this work.

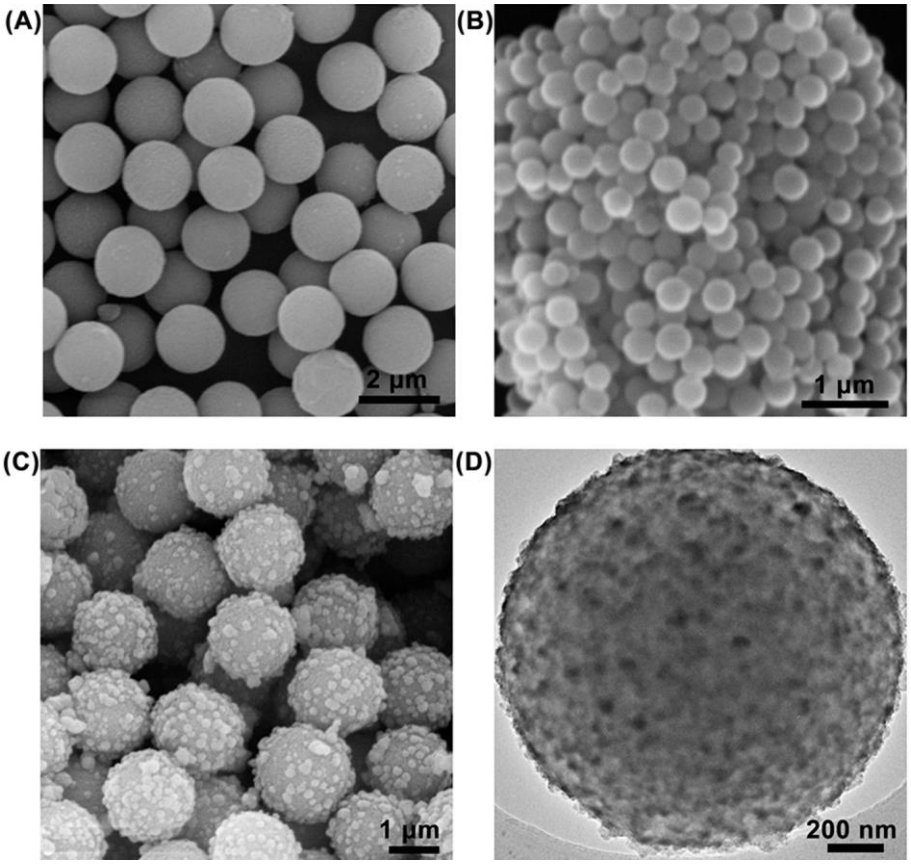


**Figure S1.** SEM images of (A) the MF and (B) MF-900. (C) SEM and (D) TEM images of the MOOH/MF.

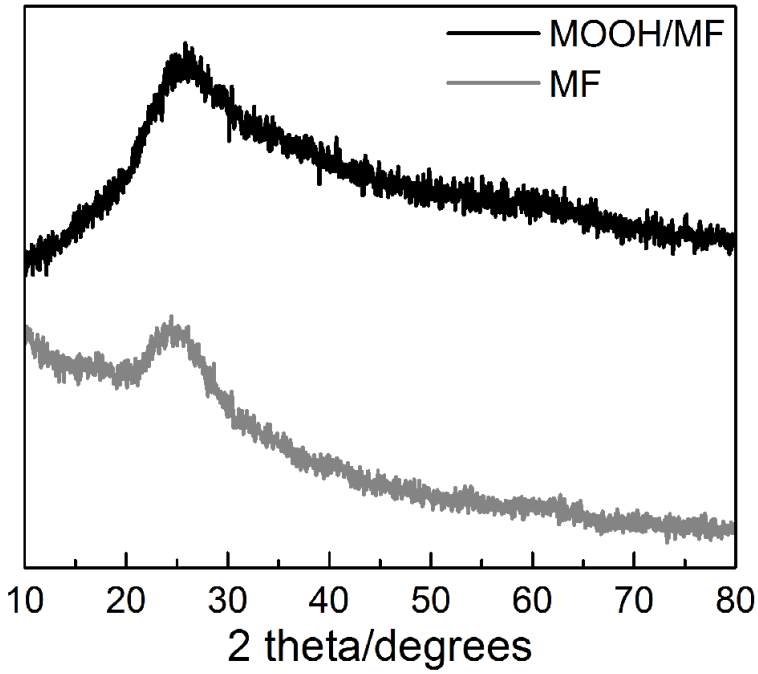


**Figure S2.** XRD patterns of the MOOH/MF and MF.

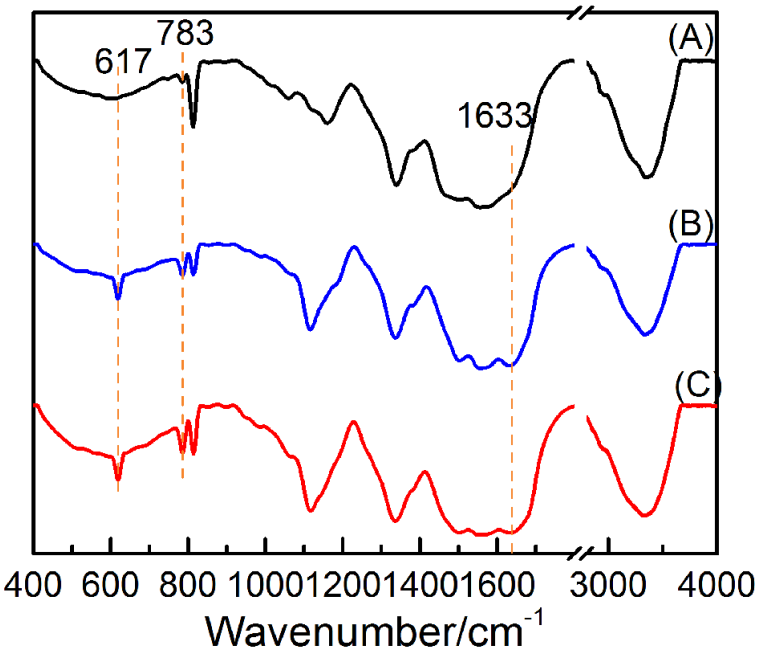


**Figure S3.** FT-IR spectra of (A) the MOOH/MF, (B) PDA-MOOH/MF, and (C) PDA/MOOH/MF.

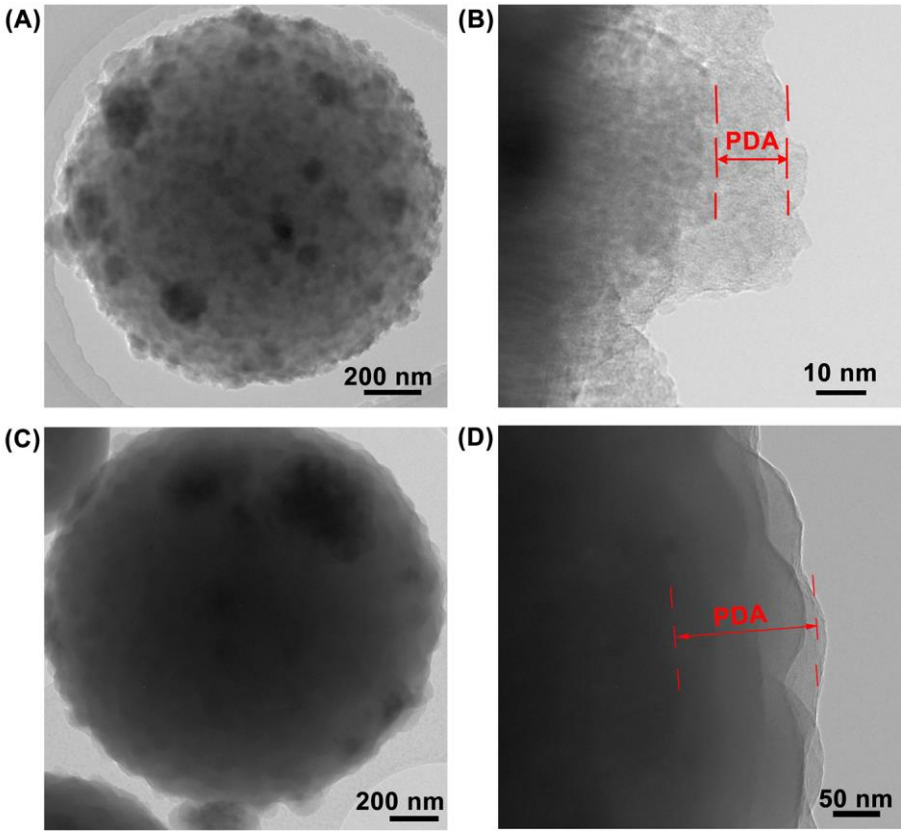


**Figure S4.** TEM images of (A, B) the PDA-MOOH/MF and (C, D) PDA/MOOH/MF.

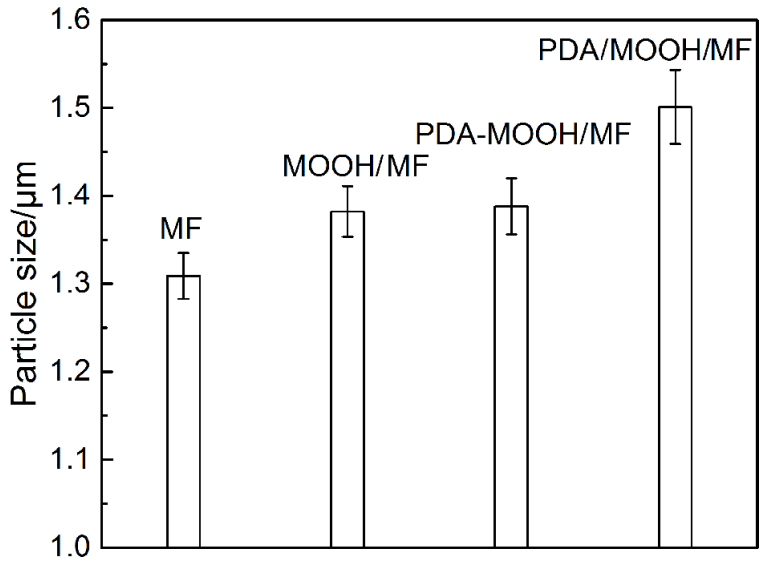


**Figure S5.** The average particle sizes of the MF, MOOH/MF, PDA-MOOH/MF, and PDA/MOOH/MF.

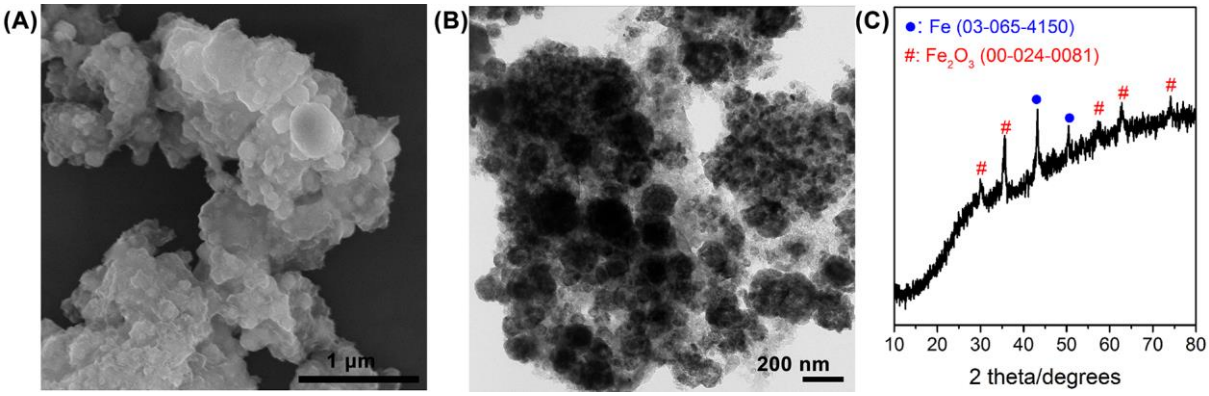


**Figure S6.** (A) SEM image, (B) TEM image, and (C) XRD pattern of the MOOH/MF-900.

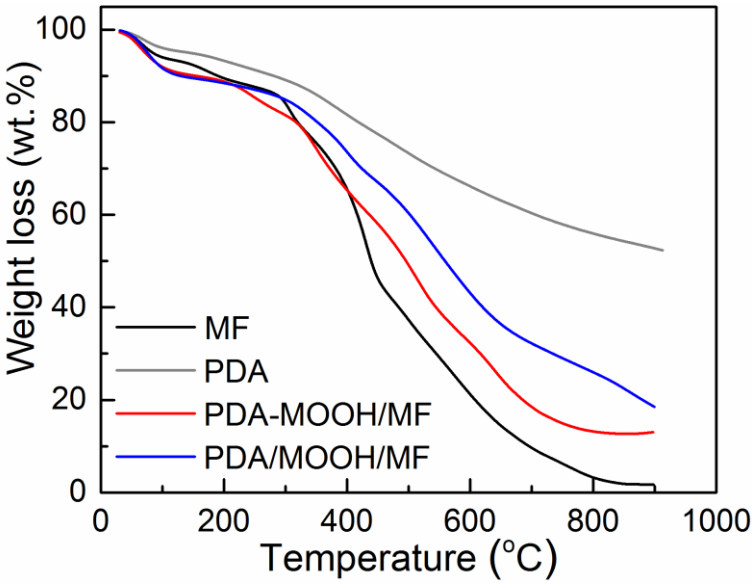


**Figure S7.** TGA curves of the MF, PDA, PDA-MOOH/MF, and PDA/MOOH/MF precursors under $N_2$ atmosphere.

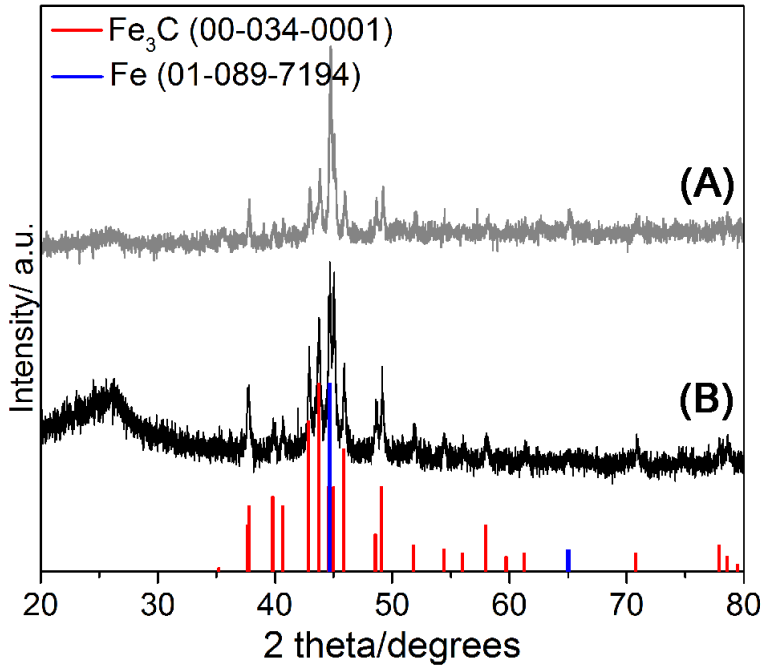


**Figure S8.** XRD patterns of (A) the PDA-MOOH/MF-900 and (B) PDA/MOOH/MF-900.

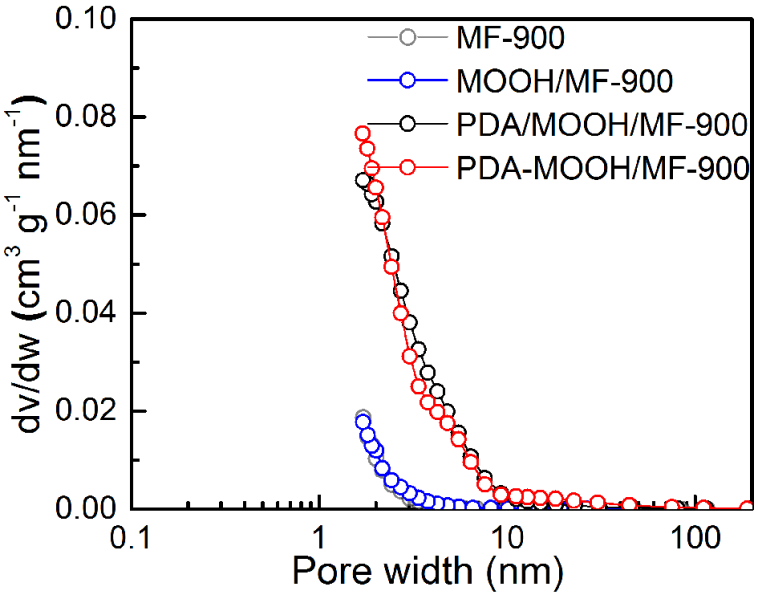


**Figure S9.** Pore size distribution curves of the MF-900, MOOH/MF-900, PDA/MOOH/MF-900, and PDA-MOOH/MF-900.

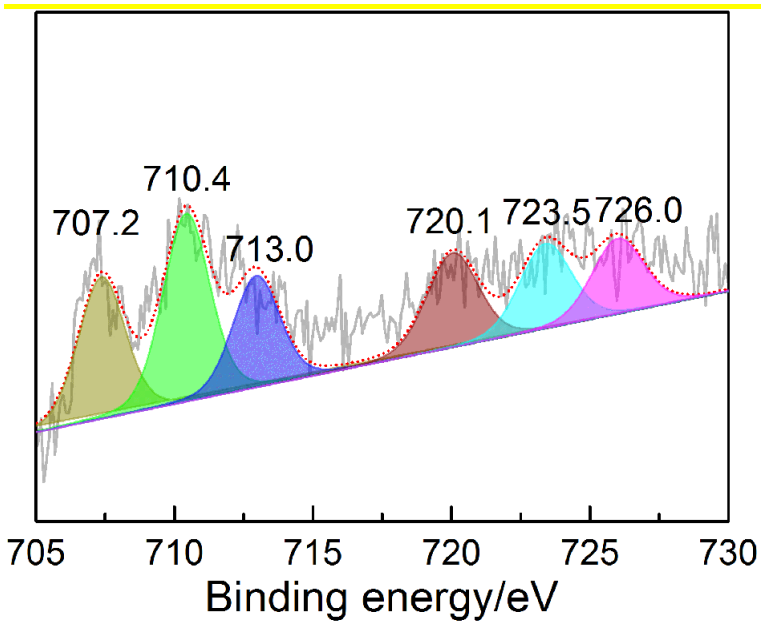


**Figure S10.** High-resolution Fe 2p XPS spectra of PDA-FeOOH/MF-900.

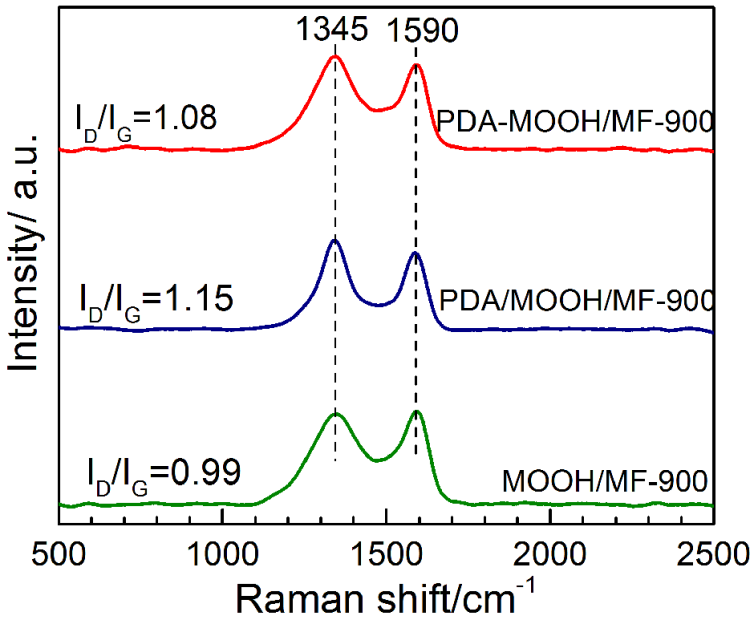


**Figure S11.** Raman spectra of the MOOH/MF-900, PDA/MOOH/MF-900, and PDA-MOOH/MF-900.

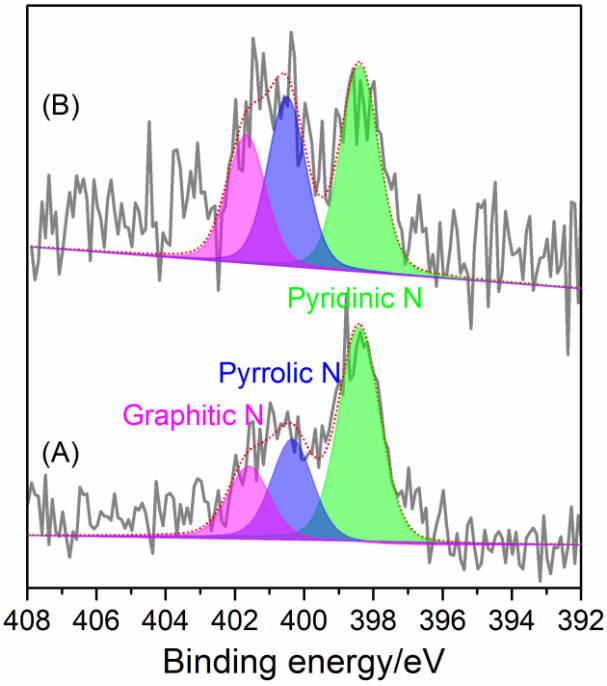


**Figure S12.** High-resolution N 1s XPS spectra of (A) the MF-900 and (B) PDA-FeOOH/MF-900.

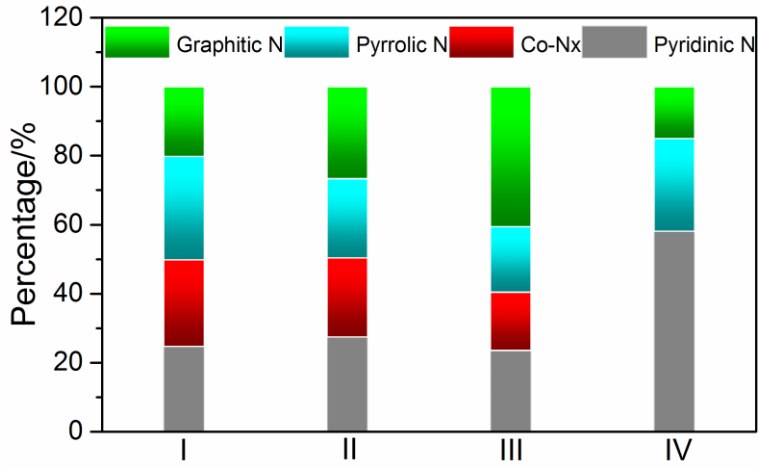


**Figure S13.** The relative percentages of pyridinic N, Co-$N_x$, pyrrolic N, and graphitic N in the PDA-MOOH/MF-900 (I), PDA/MOOH/MF-900 (II), MOOH/MF-900 (III), and MF-900 (V).

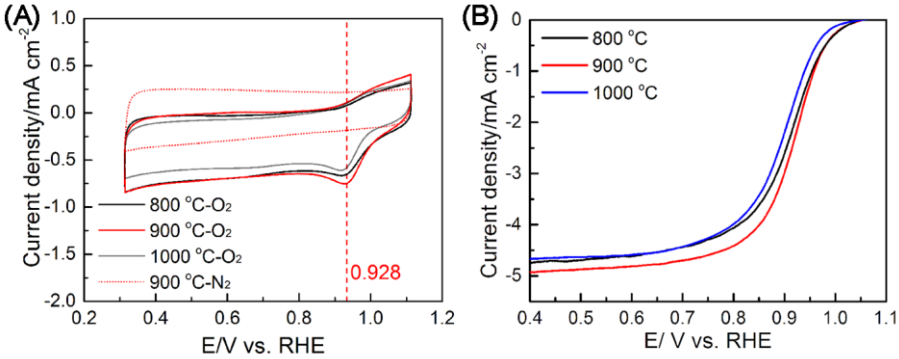


**Figure S14.** (A) CV and (B) RDE curves of the PDA-MOOH/MF-T (T=800, 900, and 1000) measured in $O_2$ or $N_2$-saturated 0.1 M KOH solution.

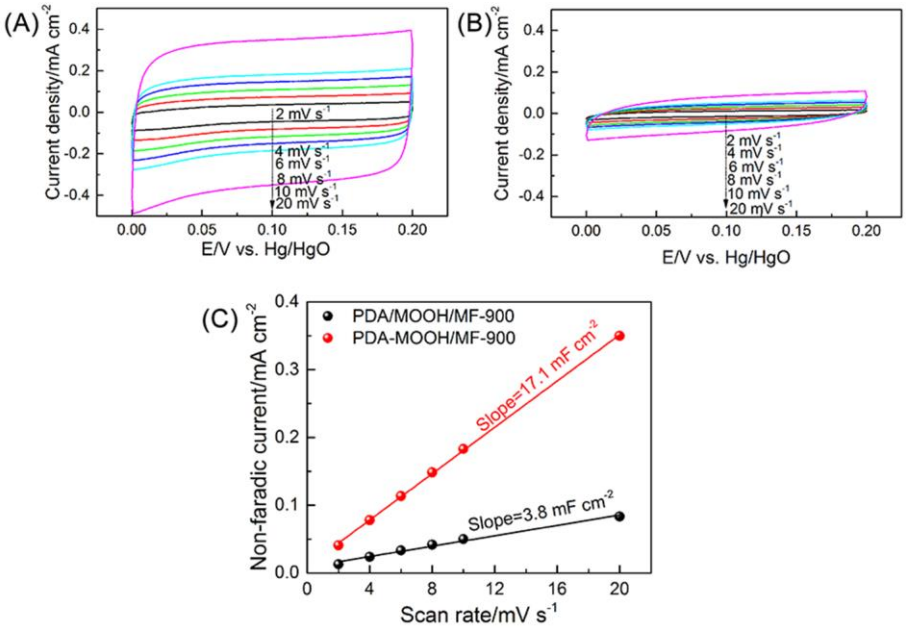


**Figure S15.** CV curves of (A) the PDA-MOOH/MF-900 and (B) PDA/MOOH/MF-900 measured in $N_2$-saturated 0.1 M KOH solution, and (C) corresponding non-Faradic current densities at 0.10 V vs. Hg/HgO versus scan rates. The measured current in non-Faradaic region is supposed to be originated from the double-layer charging. Hence, the electrochemical double-layer capacitance ($C_{dl}$) in non-Faradaic region obtained from dividing the double-layer charging current ($i_c$, mA $cm^{-2}$) by the scan rate ($\nu$, mV $s^{-1}$) is related to the electrochemically active surface area (ECSA). The specific capacitance for a flat surface ($C_s$) is estimated as 40 μF $cm^{-2}$.

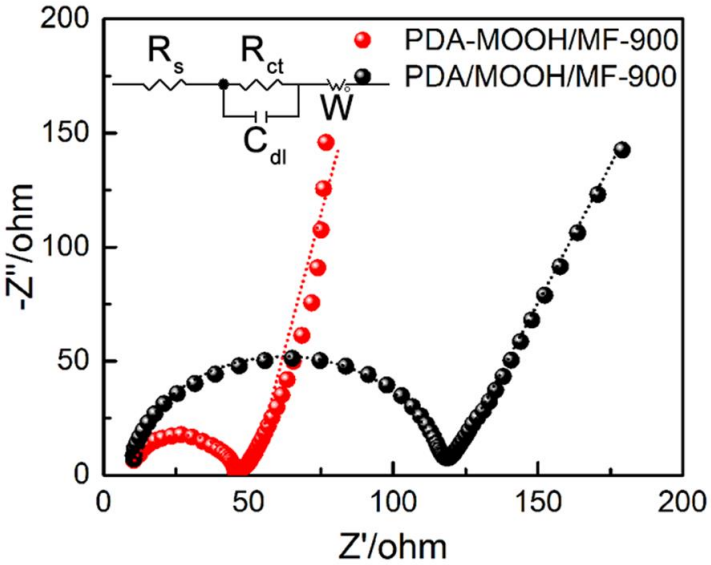


**Figure S16.** EIS spectra of the PDA-MOOH/MF-900 and PDA/MOOH/MF-900 measured in $N_2$-saturated 0.1 M KOH solution (Inset: The equivalent circuit diagram proposed for analysis of the EIS data). The EIS can be fitted into the equivalent circuit composed of the solution resistance ($R_s$), charge-transfer resistance ($R_{ct}$), double-layer capacitance ($C_{dl}$), as well as Warburg resistance (W).

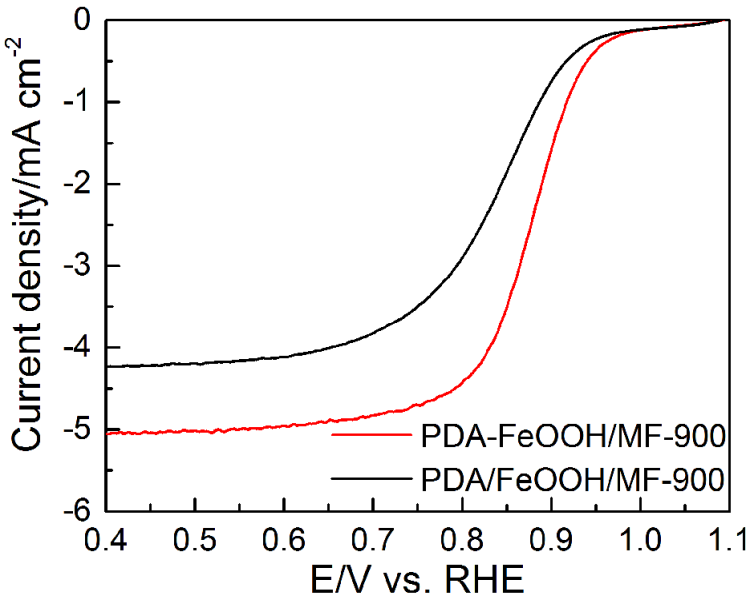


**Figure S17.** RDE curves of the PDA-FeOOH/MF-900 and PDA/FeOOH/MF-900 at 1600 rpm.

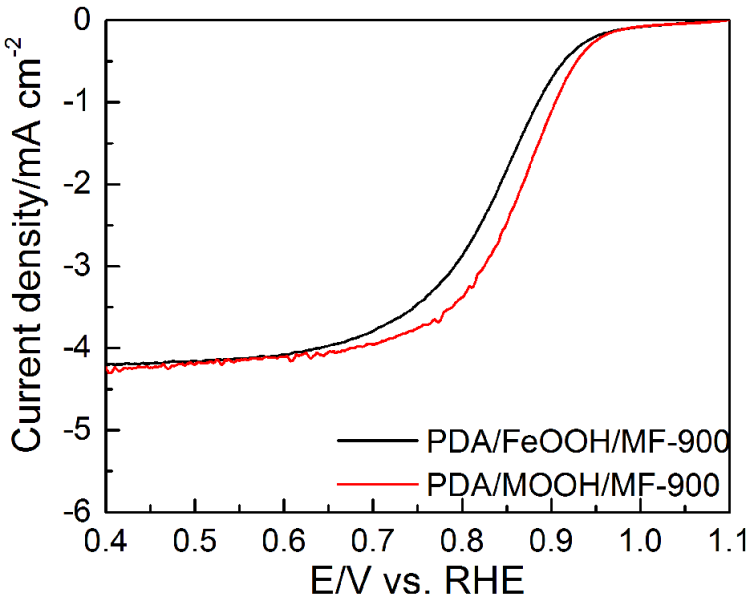


**Figure S18.** RDE curves of the PDA/FeOOH/MF-900 and PDA/MOOH/MF-900 at 1600 rpm.

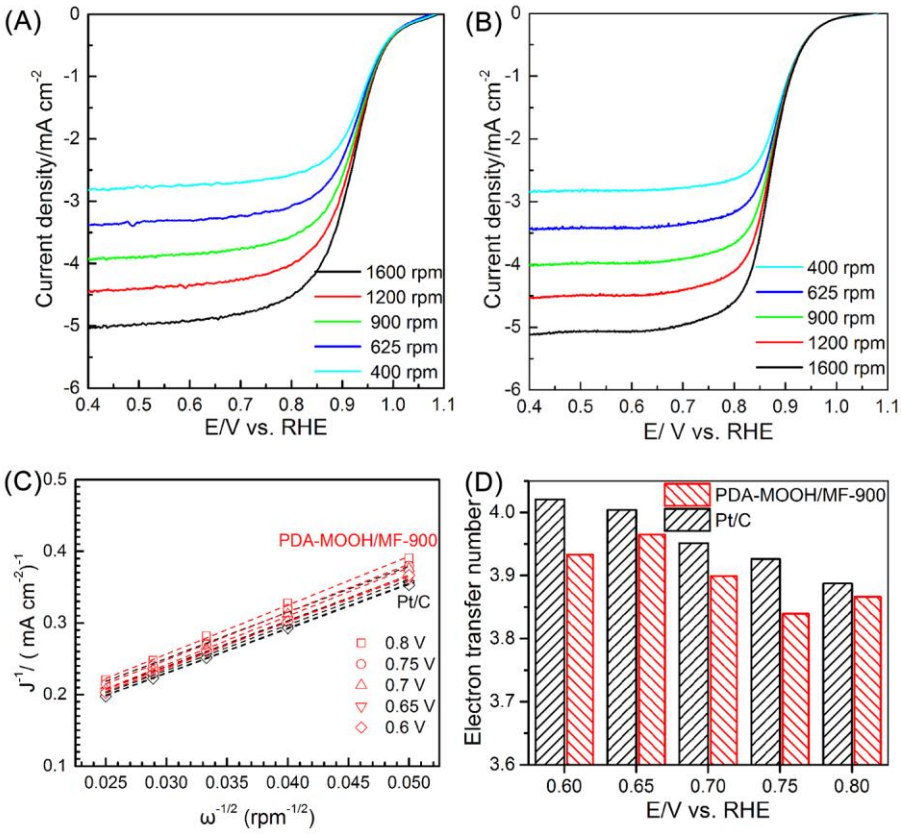


**Figure S19.** The ORR polarization curves of (A) the PDA-MOOH/MF-900 and (B) Pt/C catalysts measured in $O_2$-saturated 0.1 M KOH solution at the rotation speeds of 400-1600 rpm. (C) The K-L plots of the PDA-MOOH/MF-900 and Pt/C catalysts at 0.60-0.80 V vs. RHE and (D) corresponding electron transfer number.

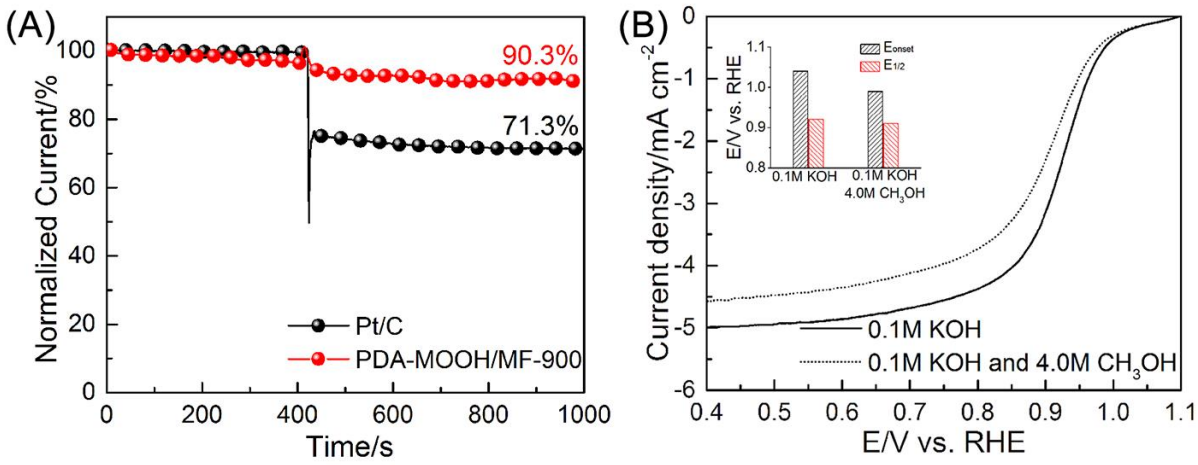


**Figure S20.** (A) Chronoamperometric curves of the PDA-MOOH/MF-900 and Pt/C catalysts at 0.50 V vs. RHE measured in $O_2$-saturated 0.1 M KOH solution upon addition of 4.0 M methanol. (B) RDE curves of the PDA-MOOH/MF-900 before and after the addition of 4.0 M methanol and (Inset) corresponding $E_{onset}$ and $E_{1/2}$ values.

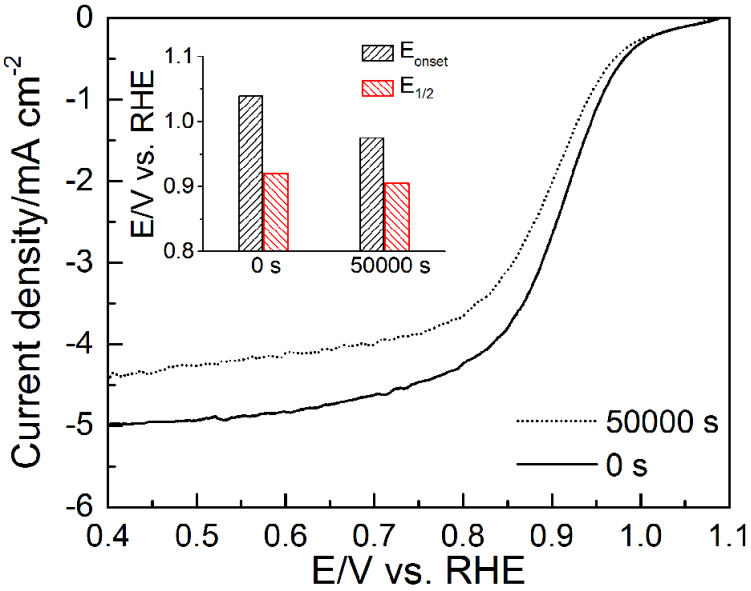


**Figure S21.** RDE curves of the PDA-MOOH/MF-900 at 1600 rpm before and after 5000 s continuous operation at 0.5 V vs. RHE and (Inset) corresponding $E_{onset}$ and $E_{1/2}$ values.

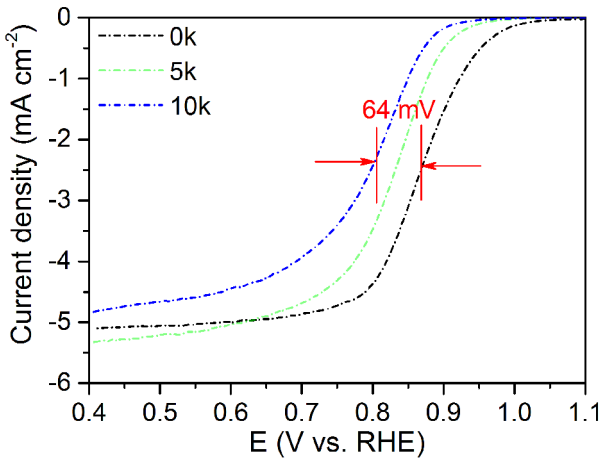


**Figure S22.** The accelerated durability tests of the Pt/C catalysts via potential cycling between 0.6 to 1.0 V vs. RHE at a scan rate of 50 mV $s^{-1}$ in $O_2$-saturated 0.1 M KOH solution.

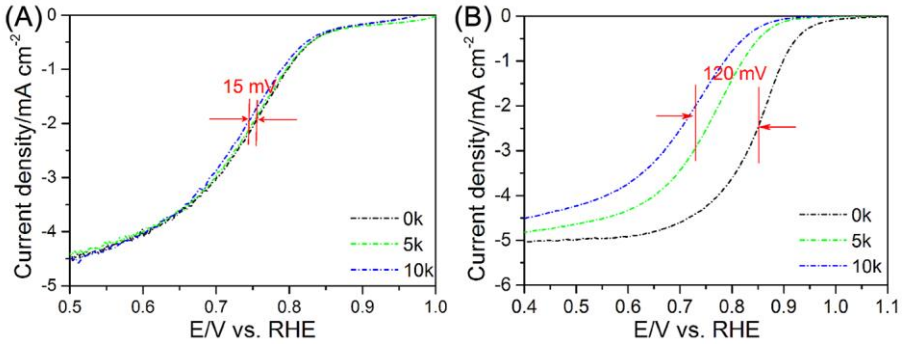


**Figure S23.** The accelerated durability tests of (A) the PDA-MOOH/MF-900 and (B) Pt/C catalysts via potential cycling between 0.6 to 1.0 V vs. RHE at a scan rate of 50 mV $s^{-1}$ in $O_2$-saturated 0.5 M $H_2SO_4$ solution.

**Table S1.** Physical Properties of preserved pulm-like PDA-MOOH/MF-900 and hollow PDA/MOOH/MF-900

| Samples | Chemical compositions | N content (at.%) [a] | Fe content (wt.%) [b] | Co content (wt.%)[b] | $I_D/I_G$[c] |
|---|---|---|---|---|---|
| PDA-MOOH/MF-900 | Fe, $Fe_3C$, Co-$N_x$/C, N-doped carbon | 2.2 | 36.76 | 0.13 | 1.08 |
| PDA/MOOH/MF-900 | Fe, $Fe_3C$, Co-$N_x$/C, N-doped carbon | 1.8 | 30.25 | 0.08 | 1.15 |

[a]: The N content is determined using XPS technique.

[b]: The Fe and Co contents are determined by using MP-AES technique.

[c]: The intensity ratio of graphitic D and G peaks in Raman spectra is measured using Raman technique.

**Table S2.** BET surface area ($S_{BET}$ $m^2$ $g^{-1}$) and pore volume ($V_{mesopore}$ and $V_{micropore}$, $cm^3$ $g^{-1}$) of PDA-MOOH/MF-900, PDA/MOOH/MF-900, MOOH/MF-900, and MF-900.

| Samples | $S_{BET}$ | $V_{mesopore}$ | $V_{micropore}$ |
|---|---|---|---|
| PDA-MOOH/MF-900 | 406.3 | 0.27 | 0.13 |
| PDA/MOOH/MF-900 | 371.4 | 0.23 | 0.10 |
| MOOH/MF-900 | 99.0 | 0.02 | 0.04 |
| MF-900 | 109.3 | 0.01 | 0.05 |

**Table S3.** Mössbauer Parameters for the PDA-MOOH/MF-900 measured at room temperature.

| Peaks | $\delta^a$ (mm/s) | $H_{hf}{}^b$ (KOe) | $\Delta E^c$ (mm/s) | $\Gamma/2^d$ (mm/s) | Area (%) | Assign |
|---|---|---|---|---|---|---|
| Single | -0.07 | | | 0.2 | 23.5 | γ-Fe |
| Sext1 | -0.04 | 331.3 | -0.11 | 0.2 | 13.1 | α-Fe |
| Sext2 | 0.19 | 207.4 | -0.03 | 0.2 | 63.4 | $Fe_3C$ |

[a]: Isomer shift

[b]: Half-width hyperfine field

[c]: Quadrupole splitting

[d]: Full width at half maximum